

Amplifying Human Strength Through a Virtual Sprung Inertia

Anthony Petrkian, Zachary Bucknor-Smartt, Crystal Q. Scott, and Gray C. Thomas

Abstract—While better known for their ability to work autonomously in structured tasks, robots have the potential to aid human workers in unstructured tasks via force control. More specifically, cobots and exoskeletons that physically interact with human operators can amplify human strength by feeding back measurements of their interaction forces, agnostic to the task the operator is performing. However, due to limited control bandwidth and coupled human–robot dynamics, naive force-feedback can easily result in instability similar to pilot-induced oscillation in planes. Controllers that amplify strength while also guaranteeing some stability properties have become the standard approach in the space, often at the cost of the user’s perception of a transparent system. This paper 1) extends a previously theorized virtual-mass-based exoskeleton controller to a strength-amplifying robot arm, 2) theoretically and experimentally demonstrate the improved stability properties that result from the inclusion of the virtual mass term, 3) identifies the robot’s end-effector compliance and self-deflection transfer functions, and 4) determines the extent to which the robot can reliably measure the stiffnesses of a spring-box apparatus in order to better understand its ability to identify human mechanical impedance.

I. INTRODUCTION

In demanding physical tasks, such as in rehabilitative healthcare, robots have the potential to assist or replace humans, with recent focus shifting toward assistive collaboration between humans and robots [1]. Unlike the inherently unsafe nature of older position-based control schemes [2], modern robot force sensing allows for safer physical contact in human–robot interaction. The main challenge is then to control the robot to work with humans in a desirable manner.

The paradigm of collaborative robots or “cobots” builds toward this challenge from an autonomous robotics baseline. Cobots are robots designed to share a workspace with humans, and are usually able to apply control schemes such as impedance control to ensure only safe levels of force are applied in the event of an unexpected collision or intentional handoff [3], [4]. However, since they are autonomous, they must reliably understand their role in the interaction or risk unwanted and unexpected behavior that interferes with the human. While studies have tried to design architectures that can sense/anticipate unexpected human behavior and plan accordingly, it remains a difficult task [5]. Even more difficult is helping the human operator to understand what the robot thinks is going on; a lack of transparency can understandably make the cobot a suspicious coworker.

For less structured and more physical tasks like those associated with rehabilitative environments and patient care, simple dynamic robot behaviors offer to be simpler for the operator to understand and rely less on complex robot

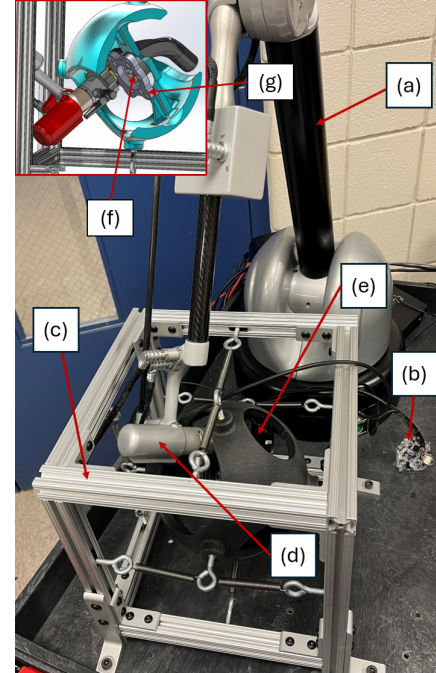


Fig. 1. The experimental setup, comprising: (a) the Haption Virtuose 6D TAO™ High Force Robotic Manipulator, (b) Sunrise Instruments (SRI) 6-axis force/torque sensor breakout board, (c) the spring-box frame, as well as the springs that attach the black sphere to the frame, (d) the end-effector of the robot arm, attached in the center of the spring-box to the black sphere, (e) the handle of the robot arm, (f) the force/torque sensor, and (g) the interface between the handle and the end-effector where the force/torque sensor is held.

decision making. Some assistive exoskeletons, for example, are attached to and directly positioned by the human as they provide assistive torque according to gravitational load of a known weight [6], acceleration of a known inertia [7], or a virtual potential energy function [8]. This removes the understanding component of the task from the robot’s responsibilities, and allows for greater flexibility for the human, provided that they can anticipate the exoskeleton’s behavior in new tasks. This assumes that the patient has some capability to perform self-movement, with the general goal to reduce the load/effort the patient needs to apply. However, these approaches are not suited for interacting with the general environments posed in rehabilitative healthcare settings, since they cannot distinguish between identical poses with different amounts of environmental interaction forces. This problem motivates the inclusion of force sensors to allow amplification of human strength in a truly task-agnostic way [9].

Feedback control of the human–robot interaction force can allow a human operator to perceive amplified strength in manipulation tasks, at least at frequencies within the

*This work supported by Texas A&M Experiment Station, the Texas Governor’s University Research Initiative, and the Texas A&M Chancellor’s University Research Initiative

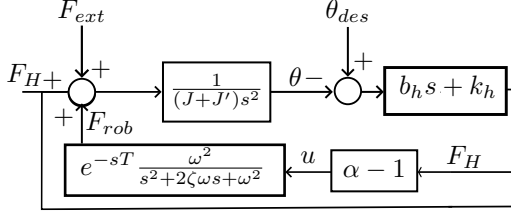


Fig. 2. Control Block Diagram: Naive Force-Feedback Controller

bandwidth of the control [9]. However, practical implementations have tended to be slow and sluggish in order to avoid instabilities in the control algorithm [10]. These instabilities (uncontrolled oscillations, etc.) are in large part due to a coupling between the exoskeleton and the human's mechanical impedance behavior [11], [12], [13], which are not unlike those found in pilot-induced oscillation [14]. Unfortunately, the human element is hard to model; they are not linear and their stiffness can change due to muscle co-contraction, fatigue, and pose [15]. Adapting to this changing behavior has required extra sensors for muscle activation and subject-specific training [16]. This means any stiffness measurements made can potentially be unreliable since they are dependent on the conditions under which the measurements occurred. Thus, even if a stiffness model is taken into account in designing the controller, amplification robots based on only force sensors are sensitive to uncontrollable stiffness changes [13], pushing designers toward low-bandwidth, conservative control tunings [17].

In this paper, we implement a controller that both amplifies human strength and adds a virtual inertia to reduce sensitivity to operator stiffness. While virtual inertia has been used before in controllers, using it for the purposes of force feedback/strength amplification is novel to this paper. More specifically, we 1) extend a previously theorized virtual-mass based energy-shaping controller approach [18] to a MIMO strength-amplifying robot arm application, 2) theoretically and experimentally demonstrate the improved stability properties that result from the inclusion of the virtual mass term, 3) identify the robot's end-effector compliance and self-deflection transfer functions, 4) validate a testing apparatus that can mimic human stiffness in multiple directions, thus allowing for experimental determination of a multi-degree-of-freedom stiffness model, and 5) experimentally validate the controller design and the robot's ability to infer the dynamics of the human surrogate. The controller is validated through comparison with a naive force-feedback approach to demonstrate the superior performance under stability constraints.

II. METHODS

A. CONTROLLER DESIGN

This paper considers two controller structures for comparison. The first, the *Naïve Controller* (Fig. 2), uses unfiltered force feedback to amplify user strength and serves as a control group in our experiment. The second, the *Virtual-*

Mass Controller (Fig. 4), applies our proposed innovation and serves as an experimental group in our experiment. Both controllers interact with the same fundamental robot physics.

1) *Plant Model*: We consider a 1-DOF linearized translational idealization of our system in which the mass of the robot, J , and any supported object, J' , are acted upon by an external force, F_{ext} , a sensed human interaction force, F_H , and a robot force F_{rob} . This model is similar to the tuning model used in [17]. Applying Newton's laws, the dynamics can be written as

$$(J + J')\ddot{\theta} = F_{rob} + F_{ext} + F_H, \quad (1)$$

where θ represents the position of the robot's end-effector, and all the forces are reflected to act in the end-effector frame.

Since the robot torque is an imperfect input that is subject to bandwidth limits, we also consider an actuator limiting transfer function,

$$\eta(s) = e^{-sT} \frac{\omega^2}{s^2 + 2\zeta\omega s + \omega^2}, \quad (2)$$

where e^{-sT} represents a time delay, and the other term is a second-order low-pass filter with critical frequency ω (bandwidth of the actuating system) and damping ratio ζ . This bandwidth limit is representative of the lowest frequency issue of the many potential bandwidth limiting effects we have not modeled, for example: electrical dynamics in the electric motor, or mechanical dynamics in the cable-drives of the robot. Including the actuator limitations, the robot force is

$$F_{rob} = \eta(s)u, \quad (3)$$

where u is the desired robot force, the input used by the feedback controller.

Thus, we consider this *open-loop* system, Σ_{open} to have three inputs (F_{ext} , F_H , and u) and one output (θ). Connecting a model for human behavior, we obtain a *human-included* system, Σ_{human} . For this purpose, we use a simple human impedance model,

$$F_H = (k_h + b_h s)(\theta_{des} - \theta), \quad (4)$$

where k_h and b_h is a human perturbation-response stiffness and damping respectively, and θ_{des} is a human desired position. The parameters k_h and b_h are not necessarily known at any given time, and are assumed to be arbitrary/allowed to take on any reasonable (positive) value. We neglect to use an inertial term, as it is only relevant at higher frequencies and is typically a very small value relative to the stiffness and damping. This system Σ_{human} is also three-input, one-output, with inputs F_{ext} , θ_{des} , and u , with output F_H .

2) *Naïve Controller*: The naïve force-feedback strength amplification controller is simple,

$$u = (\alpha - 1)F_H, \quad (5)$$

where $\alpha > 1$ is the intended amplification rate (Fig. 2). This amplification rate reflects the closed-loop dynamics resulting from the approximation $\eta(s) \approx 1$,

$$(J + J')\ddot{\theta} = F_H + (\alpha - 1)F_H + F_{ext} = \alpha F_H + F_{ext}, \quad (6)$$

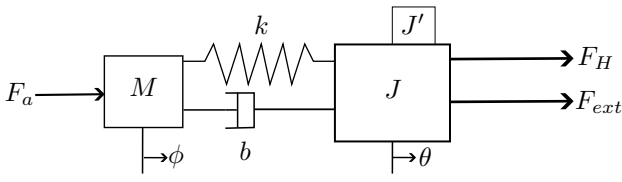


Fig. 3. FBD showing the dynamical system that would be achieved by the Virtual-Mass Controller under ideal actuation assumptions ($\eta(s) \approx 1$). The system features a virtual mass M coupled to the physical masses $J + J'$ by a virtual spring and damper. An amplification force $F_a = (\alpha - 1)F_H$ is applied to the virtual mass rather than to the physical mass in order to avoid amplification at high frequencies.

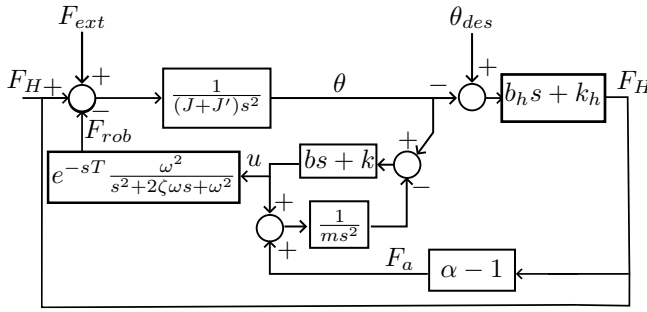


Fig. 4. Control Block Diagram: Virtual-Mass Based Controller

which shows F_H amplified by a factor of α . Naturally, such ideal behavior is not achievable with a more realistic $\eta(s)$ consideration, since it implies a meaningful change to the system dynamics at all frequencies.

3) Virtual-Mass Controller: It was previously theorized that an energy-shaping controller for exoskeletons could achieve an energetically passive mechanical interface for the human-side of an amplification behavior by simulating some specialized virtual dynamics that are coupled to the physical robot [18]. These virtual dynamics included a second copy of the robot's inertia, coupled to the physical robot by virtual springs, where the virtual inertia felt an amplified version of the human interaction force. However, the concept was only evaluated in a planar simulation of a lower-body exoskeleton with ground-contact sensing.

This paper explores a similar virtual-mass based controller for this robot arm model (Fig. 3). The dynamics of the virtual mass are denoted

$$M\ddot{\phi} = F_a + k(\theta - \phi) + b(\dot{\theta} - \dot{\phi}), \quad (7)$$

where M is the virtual mass, ϕ is the position of the virtual mass, k is the virtual spring rate, b is a virtual damper, and F_a is the ideal amplification force $F_a = (\alpha - 1)F_H$. This virtual system then imparts a force F_{rob} on the physical system using the control input u (*i.e.*, it is filtered by the actuator limitation transfer function),

$$u = k(\phi - \theta) + b(\dot{\phi} - \dot{\theta}), \quad (8)$$

resulting in a two input, one output closed loop system known as $\Sigma_{virt\ con}$ (Fig. 4), with inputs F_{ext} and θ_{des} and output F_H .

4) Steady-State Analysis: Steady-state analysis shows that this new system preserves the desired amplification behavior at low frequencies. Let $\dot{\phi} = \dot{\theta} = \ddot{\theta} = \ddot{\phi} = 0$, and (1), (2), (3), (7), and (8) reduce to

$$\begin{cases} 0 = F_{ext} + F_H + k(\phi - \theta) \\ F_a = k(\phi - \theta) \end{cases}, \quad (9)$$

where $F_a = (\alpha - 1)F_H$. The resulting steady state force balance is

$$0 = F_{ext} + \alpha F_H, \quad (10)$$

as expected. The human force required to balance the arbitrary external load is therefore reduced by a factor α , and environment-side perceptions of human strength magnified by α .

5) Stability Analysis: Whether it's rehabilitation or industrial work, an unstable control system can cause unintended harm or injury to the user. Due to the human-robot interaction in strength amplification, it is important to ensure stability of the system when a human operator is present in the control loop. The goal of this section is to show that the virtual mass controller improves the potentially attainable ratio without compromising stability.

To determine the stability of the system, we consider the two input one output system,

$$\theta(s) = G_H(s)F_H(s) + G_{ext}(s)F_{ext}(s). \quad (11)$$

Assuming θ_{des} is zero, the transfer function between the human input and theta is,

$$\theta = -H(s)F_H, \text{ where } H(s) = \frac{1}{b_h s + k_h}. \quad (12)$$

Substituting (12) into (11), we attain a closed-loop SISO system experienced by the environment,

$$\theta = (1 + H^{-1}(s)G_H(s))^{-1}G_{ext}F_{ext}. \quad (13)$$

This indicates that looking at the phase margin of the open-loop transfer function $H^{-1}(s)G_H(s)$ is enough to determine stability for the closed-loop system. In this case, the phase margin is

$$PM = \angle G_H(j\omega_c) - \angle H(j\omega_c) + 180^\circ, \quad (14)$$

where ω_c is the crossover frequency such that $\|H^{-1}(j\omega_c)G_H(j\omega_c)\| = 1$.

We use Simulink (Mathworks, Natick, MA) to model the naïve and virtual mass controller approaches, with the time-delay approximated by a first-order Padé approximation and the robot actuation bandwidth represented by a second-order low-pass filter (Fig. 5). The system parameters of the simulation are found in table I. The model does not include the human feedback in order to assess the open-loop properties. For consistency, the time-delay and bandwidth for the virtual mass simulation are the same as for the naïve approach. Picking $m = (\alpha - 1)J$ ensures the virtual mass and real mass have the same acceleration in response to human inputs, since the force due to the human that the virtual mass feels is amplified by $(\alpha - 1)$.

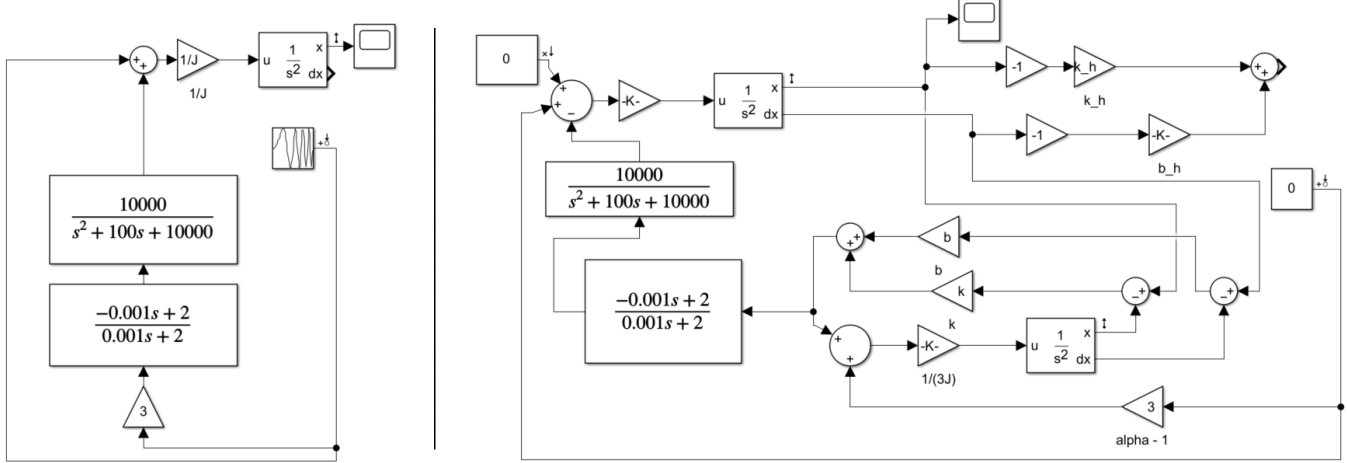


Fig. 5. Simulink model of naïve controller (left), Simulink model of virtual-mass controller (right). The model on the right shows the human model in the upper right to demonstrate how it would be included in a simulation, although it is shown to be not closed in order to assess the open-loop bode plots. The inputs are set to zero, as their value does not matter for forming the bode plots.

TABLE I
SIMULATION PARAMETERS

Parameter	Value
Strength Amplification Ratio, α	4
Time Delay, t_d	1 ms (0.001 s)
Low Pass Filter Frequency, ω_c	100 rad/s (≈ 16 Hz)
Robot Inertia (including unmodeled inertia), J	15 kg
Virtual Mass, $m = (\alpha - 1)J$	45 kg
Virtual Stiffness, k	4500 N/m
Virtual Damping, b	450 N·s/m

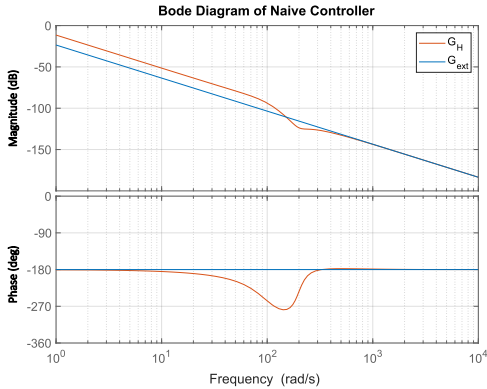


Fig. 6. Bode Plot of Naïve Controller

The Bode plot of the naïve controller system (Fig. 6) shows both the $G_{ext}(s)$ and $G_H(s)$ transfer functions. The phase of the human-side integral admittance, $G_H(s)$, for the naïve controller is either at or below -180° for the entire frequency range, with a significant phase drop to $\approx -275^\circ$ around the actuation limit/bandwidth (≈ 16 Hz). The reason for the phase drop is that at frequencies past the actuation bandwidth, the system must tend towards its natural dynamics $\frac{1}{(J+J')s^2}$. This means the transfer function representing $G_H(\frac{X}{F_H})$ must end up following the natural dynamics, and thus

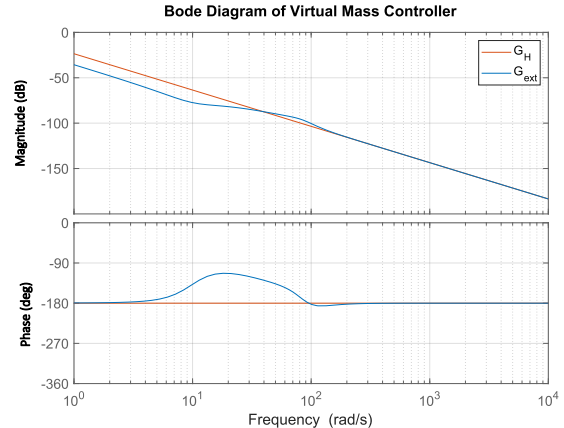


Fig. 7. Bode Plot of Virtual Mass Controller

requires a rapid drop in magnitude and phase in order to meet this requirement, as shown in the Bode plot.

Evaluating the PM from (14) for this model shows that the closed-loop SISO system risks instability if the human does not have damping, and is unstable for crossover frequencies near 16 Hz even with significant human damping. Past experiments have shown that it can be feasible for the system to be stable if the amplification ratio is small and the human stiffness is also very small (i.e. the operator is holding on loosely), however for practical purposes it is not usable.

In contrast, the Bode plot for the virtual mass controller (Fig. 7), shows a $G_H(s)$ transfer function with a constant phase of -180° , or a close approximation thereof. Rather than dropping below -180° phase like in the naïve controller, the phase for the human transfer function remains at a constant -180° , which indicates passivity. Calculating the PM from (14) with this shows that the PM will always be positive, even with the slightest human damping. This means that the controller will remain stable under any positive k_h and b_h values in the human impedance model. However, this

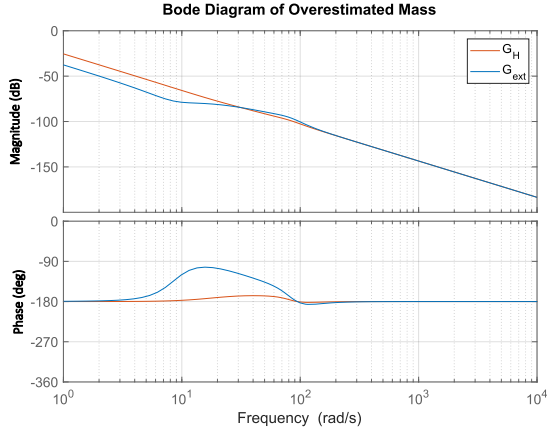


Fig. 8. Bode Plot of Overestimated Mass

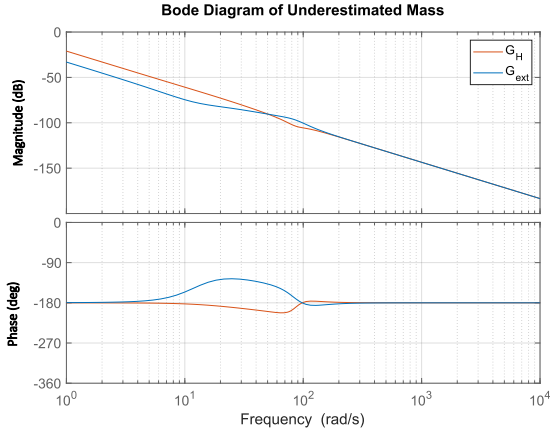


Fig. 9. Bode Plot of Underestimated Mass

comes with the assumption that J can be predicted perfectly and m chosen appropriately. The problem setup assumed an unknown inertia J' , so it is instructive to see what happens if the inertia $J + J'$ is either underestimated or overestimated in the calculation of m .

Overestimation of m (Fig. 8) maintains the positive phase margin of the system and guarantees stability of the closed-loop SISO system due to the increase in phase of the human transfer function. However, underestimation (Fig. 9) causes a noticeable phase drop below -180° in the $G_H(s)$ transfer function, although the phase drop is not as severe as that of the naive controller. Thus, over-estimating the inertia parameter m appears to be the conservative choice. Another consideration is the slight dip below -180° that the G_{ext} transfer function exhibits in the bode plots. While this is not a passive transfer function, that doesn't necessarily mean that it will exhibit unstable behavior. Since the non-passivity is due to a combination of time delay and a low-pass filter (acting as an actuation bandwidth filter), it can be shown that the passivity requirements can be relaxed for these types of systems [19].

It is instructive to think of the physics behind what is



Fig. 10. A side view of the spring box apparatus

happening. In the naive control approach, the human-side force relative to the environmental force and the robot inertia is amplified. As shown in (Fig. 6), this causes a phase drop below -180° since the artificially attenuated robot inertia must act like its natural dynamics after a certain frequency.

In the virtual mass approach, by carefully choosing the acceleration (Fig. 7), the inertia of the robot relative to the human-side remains unchanged while still amplifying the human-side force relative to the environmental force. This is why the plots in (Fig. 6) and (Fig. 7) appear switched. This maintains the stability of the closed-loop system force-feedback system. For the overestimated and underestimated robot inertia cases, they have the effect of artificially adding and decreasing the robot inertia respectively. This is why there is a small potential for instability in the underestimated case. However, the phase drop is much smaller than the naive controller and is thus less likely to be unstable. With these results, the next step is to apply these two controllers in an experiment to validate the stability analysis.

B. HARDWARE DESIGN

During this study, we deploy strength amplification controllers on the 6 degree of freedom Haption Virtuose 6D TAO™ High Force robotic manipulator (Fig. 1). Due to its low gear ratios and backdriveability, the manipulator can provide force control at its end-effector. We modify the Haption arm end-effector by integrating a 6-axis force-torque sensor between two 3D-printed plates. The plates interface with the Haption arm end-effector handle and the remaining components of the end-effector joint. This modification enables the force-torque sensor to differentiate between applied loads at the handle where the human grasps, and the end of the end-effector joint. Care was taken to ensure no force leakage could occur between the interface of the force torque sensor and the end-effector components by creating gaps between the force torque sensor and the opposing human and environment sides of the apparatus. This analysis ensured that

under maximum deflection, the two end-effector plates never collided, resulting in corrupted system identification data.

Since a major facet of strength amplification involves the coupling between the human and the robot, testing a controller can be difficult and is subject to the availability of human testing. However, this coupling is one of the major factors responsible for the instability from force-feedback, so it is necessary to have in order to test controllers in a realistic setting. One potential solution to this is to design an apparatus that can simulate human stiffness in a multiple-degree-of-freedom fashion. Not only does this allow for testing without relying on human test subjects, but it provides an avenue for testing how different stiffness values affect the controller.

We use an adjustable, spring-loaded end effector mount to simulate human arm stiffness in response to force input. Our “spring box” apparatus (Fig. 10) includes a 3D-printed PLA mount interfaces with the force torque sensor and handle on the human side. The exterior of the mount is equipped with six eye bolts secured by heat-set inserts, with each eye bolt supporting two extension springs. The springs are secured to corresponding eye bolts a long cube-shaped frame constructed from aluminum extrusion. This makes it easy to change out the springs and allows for easier testing.

In total, twelve springs in tension hold the mount in a centered equilibrium within the frame. The springs are configured such that four are oriented along each Cartesian axis. Both the spring box and the Haption arm are affixed to the same ground surface, ensuring a rigid base. The spring box was evaluated using sets of springs with rates of $k_1 = 175.13 \frac{N}{m}$, $k_2 = 437.817 \frac{N}{m}$, $k_3 = 893.146 \frac{N}{m}$, $k_4 = 1821.31 \frac{N}{m}$, and $k_5 = 4220.55 \frac{N}{m}$ which provide total spring stiffness values of $4k_n$ in each Cartesian direction.

C. SYSTEM IDENTIFICATION

We empirically identified a multi-degree-of-freedom model of the human–robot coupling dynamics using system identification. Since robot position measurements cannot be trusted in calculating the estimated stiffness of the spring box due to self-deflection of the robot, we estimated a model of this self-deflection using a chirp test with a locked end-effector. The end-effector was affixed to the table using a special purpose variant handle, and a chirp of desired end-effector frame force was applied in each Cartesian direction.

The derived compliance matrix, C_γ , is then

$$C_\gamma(\omega) = R(\omega)F_l(\omega)^{-1}, \quad (15)$$

where R is the robot’s recorded position, and F_l is the measured force via the 6-axis force-torque sensor, all as a function of frequency. After performing the locked test in all three directions, a matrix C'_γ of bode plots (Fig. 11) characterizes the compliance, and matrix inversion yields a low-frequency stiffness.

With this robot compliance model, similar chirp tests using the spring box were performed to quantify the robot’s ability to measure the mechanical impedance of the environment or human. The spring box compliance matrix, C_S , can be calculated in a similar manner to C_γ , now with a subtractive

term $(R - C_\gamma F_s)$ to extract the true end-effector position as the spring box emulates human contact,

$$C_S(\omega) = (R(\omega) - C_\gamma(\omega)F_s(\omega))F_s(\omega)^{-1}, \quad (16)$$

where R is the robot’s recorded position, and F_s is the measured force via the 6-axis force-torque sensor in the spring box test. Inverting the matrix of compliance bode plots C'_S to achieve K'_S then yields the spring box stiffness matrix, where the low-frequency response of the system represents the spring box stiffnesses mentioned previously (Fig. 6, 7).

Performing system identification on the spring box with $k_1 = 175.13 \frac{N}{m}$, $k_2 = 437.817 \frac{N}{m}$, and $k_3 = 893.146 \frac{N}{m}$ produces the following predicted stiffness matrices:

$$K_{1(N/m)} = \begin{bmatrix} 171.55 & 43.275 & 15.240 \\ 8.87 & 214.37 & 43.4172 \\ 36.11 & 87.028 & 217.57 \end{bmatrix} \quad (17)$$

$$K_{2(N/m)} = \begin{bmatrix} 257.392 & 64.877 & 63.574 \\ 125.749 & 526.829 & 137.478 \\ 282.815 & 71.431 & 538.710 \end{bmatrix} \quad (18)$$

$$K_{3(N/m)} = \begin{bmatrix} 2030.453 & 716.413 & 1659.375 \\ 235.748 & 1398.485 & 481.472 \\ 914.981 & 3536.165 & 3350.282 \end{bmatrix} \quad (19)$$

By comparing each predicted stiffness matrix with the theoretical expected stiffness matrix given by $K_i = \text{diag}(k_i, k_i, k_i)$, a Frobenius-norm error vector can be used to provide a quantitative accuracy of the prediction for each of the three tested spring stiffnesses.

$$\text{Error_Vector} = \begin{bmatrix} K_1 \text{ Error} \\ K_2 \text{ Error} \\ K_3 \text{ Error} \end{bmatrix} = \begin{bmatrix} 42.09\% \\ 55.75\% \\ 319.85\% \end{bmatrix}. \quad (20)$$

We believe the large error is most likely due to bandwidth limits in the force and position sensing, as the motion of the end-effector in the apparatus during testing is too small to have any noticeable coupling effects from the springs.

III. CONTROLLER VALIDATION EXPERIMENT

Using the spring box apparatus shown in (Fig. 10) to mimic the human stiffness shown in the control block diagrams (Fig. 2, 4), an experiment was carried out to compare the naive force-feedback controller compared to the virtual-mass based controller. The main goal of the experiment was to test stability. The amplification ratio α was chosen to be 1.5, a fairly small amount (at least for small forces). This value was picked to demonstrate that even at small amplification ratios, the naive force-feedback controller can go unstable very fast. For the virtual-mass controller, the parameter values are: $m = 5$, $k = 500$, $b = 100$.

The experiment was performed by applying the controller while the robot arm was attached to the spring box apparatus. The experimental setup is shown in (Fig. 1). After a short time, the robot arm was perturbed by a small force, and the corresponding displacement in the perturbed direction was measured. This allowed for experimentally determining stability.

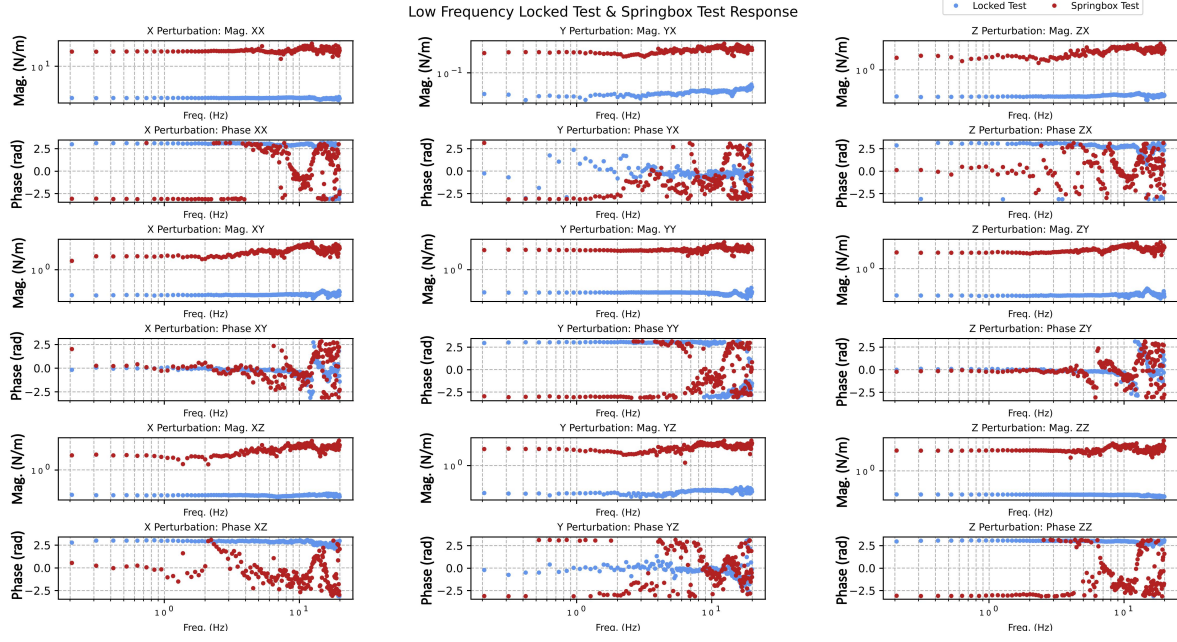


Fig. 11. Stiffness matrix of bode plots overlaying the results of the locked test as compared to the spring box test.

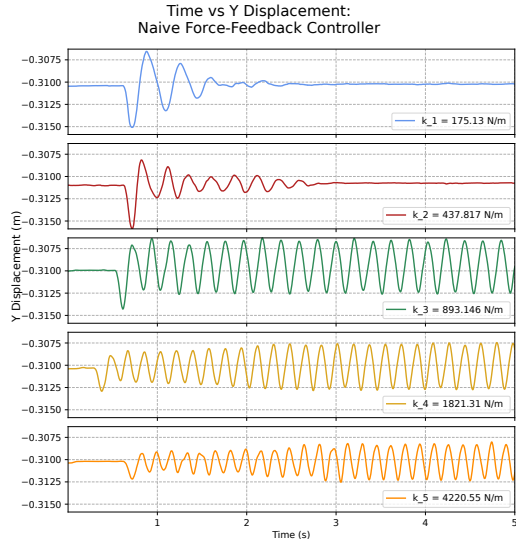


Fig. 12. Time series data of naïve force feedback control results for spring box spring constants of: $k = (175.13, 437.817, 893.146, 1821.31, 4220.55) \frac{N}{m}$ in order of top to bottom.

IV. RESULTS

The naïve controller was destabilized by increasing spring stiffness (Fig. 12), whereas the virtual-mass controller was not (Fig. 13). The naïve controller appears stable at $\alpha = 1.5$ for the first two stiffnesses ($< 500 N/m$), but sustains persistent or slowly-growing oscillations for the higher stiffness configurations of the apparatus. This demonstrates that the stability of the naïve controller is dependent on the stiffness of the human surrogate. In contrast, the virtual-mass controller shows clearly decaying perturbation responses for all five tested configurations of the apparatus (Fig. 13). As

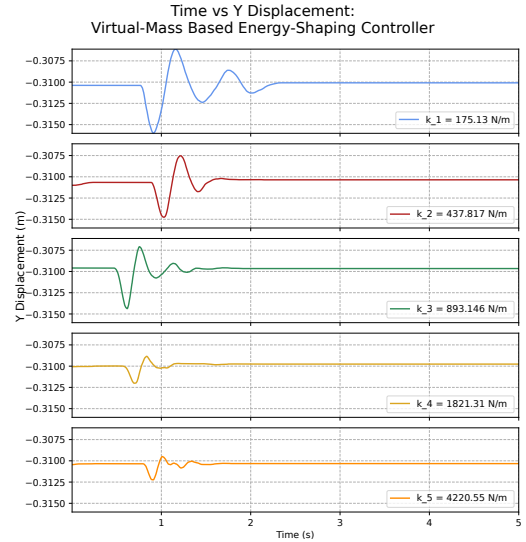


Fig. 13. Time series data of virtual-mass based force feedback control results for spring box spring constants of: $k = (175.13, 437.817, 893.146, 1821.31, 4220.55) \frac{N}{m}$ in order of top to bottom.

the spring box stiffness increased, the robot arm returned to its original position faster, which is expected of the mass-like theoretical behavior of this port (see $G_H(s)$ in Fig. 7). In comparison to the naive force-feedback tests, the virtual-mass controller showed much less oscillatory behavior for the two plots which were stable for both controllers, which is consistent with our predictions of improved phase margin.

V. DISCUSSION

Theoretically and in a simple experiment, the use of a virtual mass to reduce the environment-side admittance

reduces sensitivity to human stiffness in comparison to increasing the human-side admittance with the naïve control. Increasing the controller's estimate of the inertia furthermore allows conservative decreases in both admittances, while decreasing the controller's mass estimate smoothly transitions back toward human-side admittance increase. Notably, this result is achieved in the absence of virtual damping, a reliance on friction in the robot (none modeled in simulation), or minimum damping requirements sought from the human. While it is easy to override the dynamics of the human with a damping-based admittance controlled robot—one that only moves as fast as the human is willing to push—the approach presented here builds on an energy-conservative backdrivable robot and, with an appropriate mass estimate, does not alter the human-side dynamics of the robot relative to that behavior.

The experimental validation was, however, superficial in relation to the simulation. Only five springs were tested physically, whereas a simulated bode plot implies a stability result with all possible springs through the phase margin criterion. Future testing could reach further toward this goal if a second robot arm were available to perform frequency-domain system identification on the first arm's closed-loop behavior. In relation to the hardware, the compensation for parasitic robot compliance and torque actuation bandwidth relied on a simplifying linearization, which would need to be extended to appropriately compensate these effects throughout the workspace of the robot, and this would be a pre-condition to realistic testing with a human performing a manipulation task.

The accuracy of measurement toward the spring apparatus deteriorated for the higher stiffness configurations. This is a natural result of the increased sensitivity to the robot's imperfect compliance model when measuring stiffnesses higher than the robot's own stiffness.

Both experiment and theory stopped short of an analysis of the amplified human in feedback with a set of realistic environments. However, practical experiments suggest that interacting with the table, other humans, or small objects on the table is unlikely to destabilize either of the two tested controllers if the human grasping the handle does not. In other words, if the controller is stable under the human feedback loop, then it seems to be stable under the environmental feedback loop as well. Empirical validation of such properties might make use of yet a third robot arm for environment-side perturbation.

REFERENCES

- [1] S. Robla-Gómez, V. M. Becerra, J. R. Llata, E. González-Sarabia, C. Torre-Ferrero, and J. Pérez-Oria, "Working together: A review on safe human-robot collaboration in industrial environments," *IEEE Access*, vol. 5, pp. 26 754–26 773, 2017.
- [2] M. Vasic and A. Billard, "Safety issues in human-robot interactions," in *2013 IEEE International Conference on Robotics and Automation*, 2013, pp. 197–204.
- [3] C. Taesi, F. Aggogeri, and N. Pellegrini, "Cobot applications—recent advances and challenges," *Robotics*, vol. 12, no. 3, 2023. [Online]. Available: <https://www.mdpi.com/2218-6581/12/3/79>
- [4] B. G. C. Lima, E. Ferrentino, P. Chiacchio, and M. Vento, "Assistive force control in collaborative human-robot transportation," in *2023 32nd IEEE International Conference on Robot and Human Interactive Communication (RO-MAN)*, 2023, pp. 2646–2651.
- [5] O. C. Görür, B. Rosman, F. Sivrikaya, and S. Albayrak, "Social cobots: Anticipatory decision-making for collaborative robots incorporating unexpected human behaviors," in *Proceedings of the 2018 ACM/IEEE International Conference on Human-Robot Interaction*, ser. HRI '18. New York, NY, USA: Association for Computing Machinery, 2018, p. 398–406. [Online]. Available: <https://doi.org/10.1145/3171221.3171256>
- [6] K. Shi, J. Yang, Z. Hou, and H. Yu, "Design and evaluation of a four-dof upper limb exoskeleton with gravity compensation," *Mechanism and Machine Theory*, vol. 201, p. 105746, 2024. [Online]. Available: <https://www.sciencedirect.com/science/article/pii/S0094114X24001733>
- [7] H. Kazerooni, J.-L. Racine, L. Huang, and R. Steger, "On the control of the berkeley lower extremity exoskeleton (bleex)," in *Proceedings of the 2005 IEEE International Conference on Robotics and Automation*, 2005, pp. 4353–4360.
- [8] J. Lin, N. V. Divekar, G. C. Thomas, and R. D. Gregg, "Optimally biomimetic passivity-based control of a lower-limb exoskeleton over the primary activities of daily life," *IEEE Open Journal of Control Systems*, vol. 1, pp. 15–28, 2022.
- [9] H. Kazerooni and J. Guo, "Human Extenders," *Journal of Dynamic Systems, Measurement, and Control*, vol. 115, no. 2B, pp. 281–290, 06 1993. [Online]. Available: <https://doi.org/10.1115/1.2899068>
- [10] B. Makinson, "Research and development prototype for machine augmentation of human strength and endurance. hardiman i project," 1971. [Online]. Available: <https://api.semanticscholar.org/CorpusID:107783740>
- [11] H. Kazerooni, "Human-robot interaction via the transfer of power and information signals," *IEEE Transactions on Systems, Man, and Cybernetics*, vol. 20, no. 2, pp. 450–463, 1990.
- [12] B. He, H. Huang, G. C. Thomas, and L. Sentis, "A complex stiffness human impedance model with customizable exoskeleton control," *IEEE Transactions on Neural Systems and Rehabilitation Engineering*, vol. 28, no. 11, pp. 2468–2477, 2020.
- [13] S. P. Buerger and N. Hogan, "Complementary stability and loop shaping for improved human-robot interaction," *IEEE Transactions on Robotics*, vol. 23, no. 2, pp. 232–244, 2007.
- [14] D. T. McRuer, "Pilot-induced oscillations and human dynamic behavior," Tech. Rep., 1995.
- [15] N. Hogan, "Adaptive control of mechanical impedance by coactivation of antagonist muscles," *IEEE Transactions on Automatic Control*, vol. 29, no. 8, pp. 681–690, 1984.
- [16] H. Huang, H. F. Cappel, G. C. Thomas, B. He, and L. Sentis, "Adaptive compliance shaping with human impedance estimation," in *2020 American Control Conference (ACC)*, 2020, pp. 5131–5138.
- [17] G. C. Thomas, O. Campbell, N. Nichols, N. Brissonneau, B. He, J. James, N. Paine, and L. Sentis, "Formulating and deploying strength amplification controllers for lower-body walking exoskeletons," *Frontiers in Robotics and AI*, vol. 8, p. 720231, 2021.
- [18] G. C. Thomas and R. D. Gregg, "An energy shaping exoskeleton controller for human strength amplification," in *2021 60th IEEE Conference on Decision and Control (CDC)*, 2021, pp. 1419–1425.
- [19] G. C. Thomas, J. S. Mehling, J. Holley, and L. Sentis, "Phase-relaxed-passive full state feedback gain limits for series elastic actuators," *IEEE/ASME Transactions on Mechatronics*, vol. 26, no. 1, pp. 586–591, 2021.